


Artificial compressibility method for strongly anisothermal low Mach number flowsDorian Dupuy , Adrien Toutant,^{*} and Françoise Bataille*PROMES CNRS, Université de Perpignan Via Domitia, Rambla de la Thermodynamique, Tecnosud, 66100 Perpignan, France* (Received 12 June 2020; revised 2 January 2021; accepted 8 January 2021; published 26 January 2021)

Artificial compressibility methods aim to reduce the stiffness of the compressible Navier-Stokes equations by artificially decreasing the velocity of acoustic waves in the fluid. This approach has originally been developed as an alternative to the incompressible Navier-Stokes equations as this avoids the resolution of a Poisson equation. This paper extends the method to anisothermal low Mach number flows, allowing the simulations of subsonic flows submitted to large temperature variations, including dilatational effects. The procedure is shown to be stable and accurate using a finite-difference method in a staggered grid system for the simulation of strongly anisothermal turbulent channel flow. The highly scalable nature of the approach is well suited to complex high-fidelity simulations and GPU processing.

DOI: [10.1103/PhysRevE.103.013314](https://doi.org/10.1103/PhysRevE.103.013314)**I. INTRODUCTION**

The Mach number is an important parameter for the numerical resolution of the compressible Navier-Stokes equations with an explicit time stepping. At low Mach number, acoustic perturbations travel rapidly compared to the velocity of the fluid, such that the details of their propagation become irrelevant to the flow dynamics. At the same time, the lower the Mach number, the more acoustic waves become limiting for the time step of the simulation, severely deteriorating the efficiency of the procedure. To alleviate this restriction, low Mach number approximations of the compressible Navier-Stokes equations may be used. This includes the incompressible Navier-Stokes equations, in the absence of conduction and density gradients, and the more general low Mach number equations [1]. In both cases, no acoustic waves are generated as pressure acts within the approximate system of equations as a Lagrangian multiplier of a constraint on the divergence of velocity. Numerically, this is often resolved using at each time step a predictor-corrector projection scheme [2,3]. This operation is computationally expensive and accounts for a predominant part of the simulation cost. Several alternative approaches have been suggested to simulate incompressible flows. For instance, the lattice-Boltzmann (LB) method addresses this issue by resolving the Boltzmann transport equation on a discretized phase space [4]. The strategy followed in this paper is the use of artificial pressure equations to generate artificial acoustic waves traveling at a lower speed without affecting the velocity of the fluid. This type of approach preserves the explicit in time and local in space nature of the compressible Navier-Stokes equations, and is thus massively parallelizable and has low memory requirements. Artificial compressibility methods can be attributed to the pioneering work of Chorin [5] in the context of steady flows. The

approach can be extended to unsteady flows using a dual time-stepping procedure to enforce the incompressibility constraint at each time step, but it can also be used without subiteration [6]. The latter approach includes the α -transformation of O'Rourke and Bracco [7], the pressure gradient scaling (PGS) method of Ramshaw *et al.* [8], the acoustic speed reduction (ASR) method of Wang and Trouvé [9], the kinetically reduced local Navier-Stokes (KRLNS) equations of Ansumali *et al.* [10] and Karlin *et al.* [11], the artificial acoustic stiffness reduction method (AASCM) of Salinas-Vázquez *et al.* [12], the entropically damped artificial compressibility (EDAC) method of Clausen [13], and the general pressure (GP) equation of Toutant [14]. These methods provide successive improvements to the numerical simulation of incompressible flows using artificial pressure equations, and they have been validated extensively for both laminar and turbulent viscous flows in the literature [11,13,15–18]. To the best of our knowledge, low Mach number flows with large temperature variations have been relatively ignored up to now in these developments despite their ubiquitousness in a large variety of industrial applications, including heat exchangers, propulsion systems, or nuclear or concentrated solar power plants [19–22]. Strongly anisothermal low Mach number flows suffer from the same time-step restrictions as incompressible flows using the compressible Navier-Stokes equations, and they would also greatly benefit from the performance and scalability improvements provided by artificial compressibility methods. However, this type of flow is governed by a strong coupling between temperature and velocity [23–26] and thus it cannot be resolved by including the temperature as a passive scalar in existing methods.

In this paper, we develop an artificial compressibility method suited to anisothermal flows, and we validate the approach for a strongly anisothermal turbulent channel flow. A derivation of the artificial compressibility equations is presented in Sec. II. The relevance of the procedure is then verified numerically in Sec. III.

^{*}Author to whom all correspondence should be addressed: adrien.toutant@univ-perp.fr

II. DERIVATION OF AN ANISOTHERMAL ARTIFICIAL COMPRESSIBILITY METHOD

To derive a system of equations for anisothermal low Mach number flows, the present paper uses a two-step procedure, in which the Mach number of the flow is first increased through a modification of the initial and boundary conditions and then artificially reduced using a change of variable in order to recover the original initial and boundary conditions of the system while preserving the ratio between the fluid velocity and the speed of sound. The procedure is motivated by the fact that, with an explicit time-stepping method, the number of time steps required to simulate a flow time is lower at larger Mach number. To determine the effect of Mach number variations on the flow variables, the asymptotic development of the compressible Navier-Stokes equations as a function of the squared Mach number is used, introducing two pressures: the thermodynamic pressure and the mechanical pressure.

Let us assume for this purpose a flow that can be modeled in the immobile bounded domain Ω of volume V using the compressible Navier-Stokes equations without body forces or heat sources and the ideal gas equation of state,

$$\frac{\partial \rho}{\partial t} + \frac{\partial \rho u_j}{\partial x_j} = 0, \quad (1)$$

$$\frac{\partial \rho u_i}{\partial t} + \frac{\partial \rho u_j u_i}{\partial x_j} = -\frac{\partial p}{\partial x_i} + \frac{\partial \sigma_{ij}}{\partial x_j}, \quad (2)$$

$$\frac{\partial p}{\partial t} + \frac{\partial u_j p}{\partial x_j} = -(\gamma - 1) \frac{\partial q_j}{\partial x_j} + p(1 - \gamma) \frac{\partial u_j}{\partial x_j}, \quad (3)$$

$$p = r\rho T, \quad (4)$$

where ρ is the density, t is the time, p is the pressure, γ is the adiabatic index of the fluid, r is the ideal gas specific constant, u_i is the i th component of velocity, and x_i is the Cartesian coordinate in the i th direction. The shear-stress tensor σ and the conductive heat flux q are assumed to be of the form $\sigma_{ij} = \mu(T)[(\partial_j u_i + \partial_i u_j) - (2/3)\partial_k u_k \delta_{ij}]$ and $q_j = -\lambda(T)\partial_j T$, respectively, where the dynamic viscosity $\mu(T)$ and the heat conductivity $\lambda(T)$ are functions of temperature. For simplicity, we neglect the dissipation in the pressure evolution equation (3) as this term vanishes in the low Mach number limit. The flow is characterized by a density scale ρ^b , a velocity scale u^b , and a pressure scale p^b . The nondimensional numbers associated with the flow are the Reynolds number $\text{Re} = \rho^b u^b x^b / \mu(T^b)$, the Prandtl number $\text{Pr} = \mu(T^b)C_p / \lambda(T^b)$, and the Mach number $\text{Ma} = u^b / c^b$, with x^b a length scale characterizing the geometry, C_p is the isobaric heat capacity of the fluid, and $c^b = \sqrt{\gamma r T^b}$ is the typical velocity of acoustic waves.

As a first step, we assume that this initial flow can be approximated, in a nondimensionalized sense, by another flow defined on the same domain Ω and length scale x^b but with a larger Mach number αMa , where $\alpha > 1$ is a speedup factor. This is justified by the fact that, if the Mach number Ma of this initial flow is sufficiently small, the larger Mach number αMa is also small. The Mach number can be modified through a modification of either the velocity scale or the temperature scale of the flow. To avoid dealing with the dependence of viscosity and thermal conductivity on temperature, we choose to preserve the temperature scale of the flow. To determine

how velocity, density, and pressure should be transformed, an asymptotic development of the nondimensionalized variables involved in the compressible Navier-Stokes equations as a function of the squared Mach number can be used [27]. At low Mach number, the nondimensionalized density and velocity are independent of the Mach number, while the Mach number dependence of pressure cannot be neglected. Namely, $u/u^b \approx \hat{u}_0$, $\rho/\rho^b \approx \hat{\rho}_0$, and $p/p^b \approx \hat{p}_0 + \text{Ma}^2 \hat{p}_1$, where \hat{u}_0 , $\hat{\rho}_0$, \hat{p}_0 , and \hat{p}_1 do not depend on the Mach number. The zeroth-order nondimensionalized pressure \hat{p}_0 can be shown to be constant in space by injecting these asymptotic developments into the Navier-Stokes equations [27–29]. It is therefore useful to decompose pressure in a thermodynamic pressure $p_0 = p^b \hat{p}_0$ and a mechanical pressure $p_1 = p - p_0 = p^b \text{Ma}^2 \hat{p}_1$. Let us consider, using this definition, that the initial flow is characterized by the tuple $F(\mathbf{x}, t) = (\rho(\mathbf{x}, t), u(\mathbf{x}, t), p_0(t), p_1(\mathbf{x}, t))$ governed by Eqs. (1)–(4) along with a set of initial conditions $F_i(\mathbf{x}) = (\rho_i(\mathbf{x}), u_i(\mathbf{x}), p_{0i}, p_{1i}(\mathbf{x}))$, such that $F(\mathbf{x}, 0) = F_i(\mathbf{x})$, and a set of boundary conditions $F_b(\mathbf{x}, t) = (\rho_b(\mathbf{x}, t), u_b(\mathbf{x}, t), p_{0b}(t), p_{1b}(\mathbf{x}, t))$, such that $\mathcal{D}F(\mathbf{x}, t) = \mathcal{D}F_b(\mathbf{x}, t)$ on the boundary $\partial\Omega$ of Ω , where \mathcal{D} is a differential operator. The flow with a larger Mach number αMa may in that case be defined by using a time scale $t^b = t^b/\alpha$, a density scale $\rho^b = \rho^b/\alpha$, a velocity scale $u^b = \alpha u^b$, and a pressure scale $p^b = p^b/\alpha$. The corresponding thermodynamic mechanical pressures are $p'_0 = p^b \hat{p}_0 = p_0/\alpha$ and $p'_1 = p^b \alpha^2 \text{Ma}^2 \hat{p}_1 = \alpha p_1$. In other words, it is characterized by the tuple $F'(\mathbf{x}, t') = (\rho'(\mathbf{x}, t'), u'(\mathbf{x}, t'), p'_0(t'), p'_1(\mathbf{x}, t'))$, governed by Eqs. (1)–(4) along with the initial conditions $F'_i(\mathbf{x}) = (\rho_i(\mathbf{x})/\alpha, \alpha u_i(\mathbf{x}), p_{0i}/\alpha, \alpha p_{1i}(\mathbf{x}))$, and the boundary conditions $F'_b(\mathbf{x}, t') = (\rho_b(\mathbf{x}, t')/\alpha, \alpha u_b(\mathbf{x}, t'), p_{0b}(t')/\alpha, \alpha p_{1b}(\mathbf{x}, t'))$. Indeed, the resulting flow has the same Reynolds number $\text{Re}' = \rho^b u^b x^b / \mu(T^b) = \text{Re}$ and Prandtl number $\text{Pr}' = \mu(T^b)C_p / \lambda(T^b) = \text{Pr}$ as the flow F but a larger Mach number $\text{Ma}' = u^b/c^b = \alpha \text{Ma}$.

As a second step, the variables of the sped-up flow F' are transformed to embed the modifications of the initial and boundary conditions within the system of equations. This change of variable should counteract the above speedup of the flow. By introducing $t'' = \alpha t'$, $u'' = u'/\alpha$, $\rho'' = \alpha \rho'$, $p''_0 = \alpha p'_0$, and $p''_1 = p'_1/\alpha$ into Eqs. (1)–(4), the flow F' is associated with an artificial flow F'' , described by the set of governing equations

$$\frac{\partial \rho''}{\partial t''} + \frac{\partial \rho'' u''_j}{\partial x_j} = 0, \quad (5)$$

$$\frac{\partial \rho'' u''_i}{\partial t''} + \frac{\partial \rho'' u''_j u''_i}{\partial x_j} = -\frac{\partial p''_1}{\partial x_i} + \frac{\partial \sigma''_{ij}}{\partial x_j}, \quad (6)$$

$$\frac{\partial p''_1}{\partial t''} + \frac{\partial u''_j p''_1}{\partial x_j} = -\frac{(\gamma - 1) \partial q_j}{\alpha^2 \partial x_j} + \left(p''_1(1 - \gamma) - \frac{\gamma p''_0}{\alpha^2} \right) \times \frac{\partial u''_j}{\partial x_j} - \frac{1}{\alpha^2} \frac{\partial p''_0}{\partial t''}, \quad (7)$$

$$p''_0 + \alpha^2 p''_1 = r\rho'' T, \quad (8)$$

where the fact that the thermodynamic pressure p''_0 is constant in space is used to simplify Eqs. (6) and (7). The

corresponding initial conditions, $F_i''(\mathbf{x}) = F_i(\mathbf{x})$, and boundary conditions, $F_b''(\mathbf{x}, t'') = F_b(\mathbf{x}, t)$, are identical to those of the initial flow. Accordingly, since the two pressures p_0'' and p_1'' approximate the two pressures p_0 and p_1 of the initial flow, respectively, the “full” pressure p of the initial flow is best approximated by $p'' = p_0'' + p_1''$, which does not obey the equation of state (8). To close the system of equations, notice first that any global variations of mechanical pressure can be absorbed into thermodynamic pressure without changing the equations. This may be shown, for instance, by decomposing pressure in a mean pressure $\bar{p}'' = p_0'' + (\alpha^2/V) \int_{\psi} p_1'' dV$ and a fluctuating pressure $\dot{p}'' = p_1'' - (1/V) \int_{\psi} p_1'' dV$ in Eqs. (5)–(8). With this decomposition, the “full” pressure would be approximated as $p \approx \bar{p}'' + \dot{p}'' = p_0'' + p_1'' + [(\alpha^2 - 1)/V] \int_{\psi} p_1'' dV$, which introduces a small error compared to the above decomposition. For clarity, we keep the notations p_0'' and p_1'' and assume henceforth that the volume integral of p_1'' is zero. Equation (7) can with these notations be integrated to provide an equation for p_0'' , closing the system:

$$\begin{aligned} \frac{\partial p_0''}{\partial t''} = & - \underbrace{\frac{\alpha^2}{V} \int_{\partial\Omega} p_1'' u_j'' n_j dS - \frac{\gamma p_0''}{V} \int_{\partial\Omega} u_j'' n_j dS}_{(I)} \\ & - \underbrace{\frac{(\gamma - 1)}{V} \int_{\partial\Omega} q_j n_j dS}_{(II)} + \underbrace{\frac{\alpha^2(1 - \gamma)}{V} \int_{\Omega} p_1'' \frac{\partial u_j''}{\partial x_j} dV}_{(III)}, \end{aligned} \quad (9)$$

with \mathbf{n} the outward-pointing unit normal vector to the surface $\partial\Omega$. Note that if a more accurate prediction of the “full” pressure is deemed important, for instance in the case of the dependence of the fluid properties on pressure, the time derivative of p_1'' can alternatively be included in Eq. (9). The system of Eqs. (5)–(9) produces acoustic waves with a velocity artificially reduced by a factor α^2 compared to the original system [(1)–(4)]. It is accordingly more efficient to resolve with an explicit time-stepping method. Note that although $\alpha > 1$ for the purpose of artificial compressibility methods, the above developments are also valid for low values of α . In particular, the system of Eqs. (5)–(9) tends to the low Mach number equations of Paolucci [1] as α tends to zero and the velocity of acoustic waves tends to infinity. In that case, the time derivative of p_1 becomes negligible in front of the dilatation and conduction terms in Eq. (7) as α tends to zero. Equation (7) thus becomes a constraint on the divergence of velocity that needs to be resolved at each time step to determine p_1 .

The present method is proposed as an alternative to the resolution of the low Mach number equations [1], in which no acoustic waves are generated, and it targets the same type of strongly anisothermal low Mach number flows. Although thermoacoustic waves [30] are produced by the system of equations, the method is not expected to be relevant to their study as their velocity has been reduced artificially. Compared to the artificial methods devised for incompressible flows [11,13,14,18], the proposed methodology includes two pressures in the final set of Eqs. (5)–(9), namely the thermodynamic pressure and the mechanical pressure. This

decomposition is useful to take into account anisothermal effects because the two pressures are affected differently by a reduction of the speed of sound. In addition, thermal conduction must be properly scaled by $1/\alpha^2$ in Eq. (7) to account for Mach number effects. The first two terms (I) and (II) of Eq. (9) are surface averages and thus typically inexpensive to compute. In addition, they vanish in isolated systems or if the inward and outward fluxes cancel out. The third term (III) is related to flow dilatation and can be expected to be small since this correlation is usually very small in low Mach number flows [25,31]. The validity of this assumption will be discussed in more detail in the following. The convective term in Eq. (7) has been found to be crucial for incompressible flows in a previous paper [18]. The diffusive term in Eq. (7) physically represents thermal conduction and may thus not be neglected in the case of strongly anisothermal flows that are the target of this study. Similarly, numerical evidence (not presented here) shows that the term $\alpha^2 p_1''$ in the ideal gas Eq. (8) cannot be neglected, as would be the case in the low Mach number approximation [1].

III. RESULTS

The use of the artificial pressure Eqs. (5)–(9) to simulate anisothermal low Mach number flows is demonstrated using a fully developed turbulent anisothermal channel flow. The configuration is composed of a two no-slip plane walls at constant temperature enclosing a fully turbulent fluid flow. The bottom wall ($y = 0$) is at the temperature $T_1 = 293$ K and the top wall ($y = 2h$) is at the temperature $T_2 = 586$ K. A large temperature ratio of 2 between the hot and cold sides of the channel is selected in order to induce an asymmetry between the hot and cold sides of the channel. The actual value of the wall temperature does not affect the validity of the artificial compressibility assumption, provided that the Mach number is fixed, but it can influence the validity of other modeling assumptions (ideal gas law, Sutherland’s law). The streamwise (x) and spanwise (z) directions are periodic and statistically homogeneous. The Richardson number $Ri = Gr/Re^2$ is small ($Ri \approx 0.01$) as the distance between the top and bottom walls is small and gravity acts perpendicularly to the flow direction, as is the case in a beam-down solar receiver. A forced convection regime where buoyancy is neglected can thus be assumed. The flow is characterized by the Prandtl number and the mean friction Reynolds number $Re_{\tau} = (1/2)(Re_{\tau,1} + Re_{\tau,2})$, where $Re_{\tau,1}$ and $Re_{\tau,2}$ are, respectively, the friction Reynolds number at the bottom and hot wall, defined as

$$Re_{\tau,\omega} = \frac{u_{\tau,\omega} h}{\nu_{\omega}}, \quad (10)$$

with ν_{ω} the kinematic viscosity and $u_{\tau,\omega} = \sqrt{\nu_{\omega} (\partial_y \langle u \rangle_x)_{\omega}}$ the friction velocity at the corresponding wall. Two mean friction Reynolds numbers (180 and 395) and three Prandtl numbers (0.76, 1.0, and 3.0) are selected, as reported in Table I. In the case $Re_{\tau} = 180$ and $Pr = 0.76$, the Mach number based on the volumetric flow rate is $Ma = 0.008$, whereas the artificial Mach numbers used in the simulations are $\alpha Ma = 0.08, 0.25, 0.45, 0.55, \text{ and } 0.65$. In all other cases, a single artificial Mach number is used, corresponding to $\alpha = 10$. We used a structured mesh, regular in the directions x and z and following

TABLE I. Flow variables and numerical domain of the selected configurations. The value of the Nusselt numbers Nu_1 and Nu_2 associated with the bottom and top walls corresponds to the reference projection simulation.

Re_τ	Pr	Domain size	Grid points	Nu_1	Nu_2	Ma	α Ma
180	0.76	$4\pi h \times 2h \times 2\pi h$	$48 \times 50 \times 48$	6.0	4.2	0.008	0.08, 0.25, 0.45, 0.55, 0.65
180	1.0	$4\pi h \times 2h \times 2\pi h$	$48 \times 50 \times 48$	7.1	5.0	0.008	0.08
180	3.0	$4\pi h \times 2h \times 2\pi h$	$48 \times 50 \times 48$	13	9.9	0.008	0.08
395	0.76	$4\pi h \times 2h \times (4/3)\pi h$	$96 \times 100 \times 64$	12	8.9	0.018	0.18

a hyperbolic tangent law in the wall-normal direction. In the case $Re_\tau = 180$, the cell sizes in the wall units are $\Delta_x^+ = 68$, $\Delta_y^+ = 0.50$ at the wall and 25 at the center, and $\Delta_z^+ = 34$. In the case $Re_\tau = 395$, the cell sizes in the wall units are $\Delta_x^+ = 73$, $\Delta_y^+ = 0.50$ at the wall and 27 at the center, and $\Delta_z^+ = 36$. The effect of the grid size on the relevance of artificial compressibility simulations was studied in Dupuy *et al.* [18] at the isothermal limit. The mesh resolution was found to have no strong effect on the accuracy of an artificial compressibility simulation compared to a reference projection simulation on the same grid. The numerical method is based on a

finite-difference method written in a staggered grid system [32]. The time scheme is given by a semi-implicit third-order Runge-Kutta method [33]. The large temperature variations reduce the time step because of the variations of fluid properties. In the momentum conservation Eq. (6), the convective term is discretized using a fourth-order centered scheme while the diffusive term is discretized with a second-order centered scheme [25,34–37]. In the artificial pressure Eq. (7), the diffusive term and the velocity-divergence term are discretized with a second-order centered scheme [18], as described in Appendix. The convective term in the mass conservation Eq. (5)

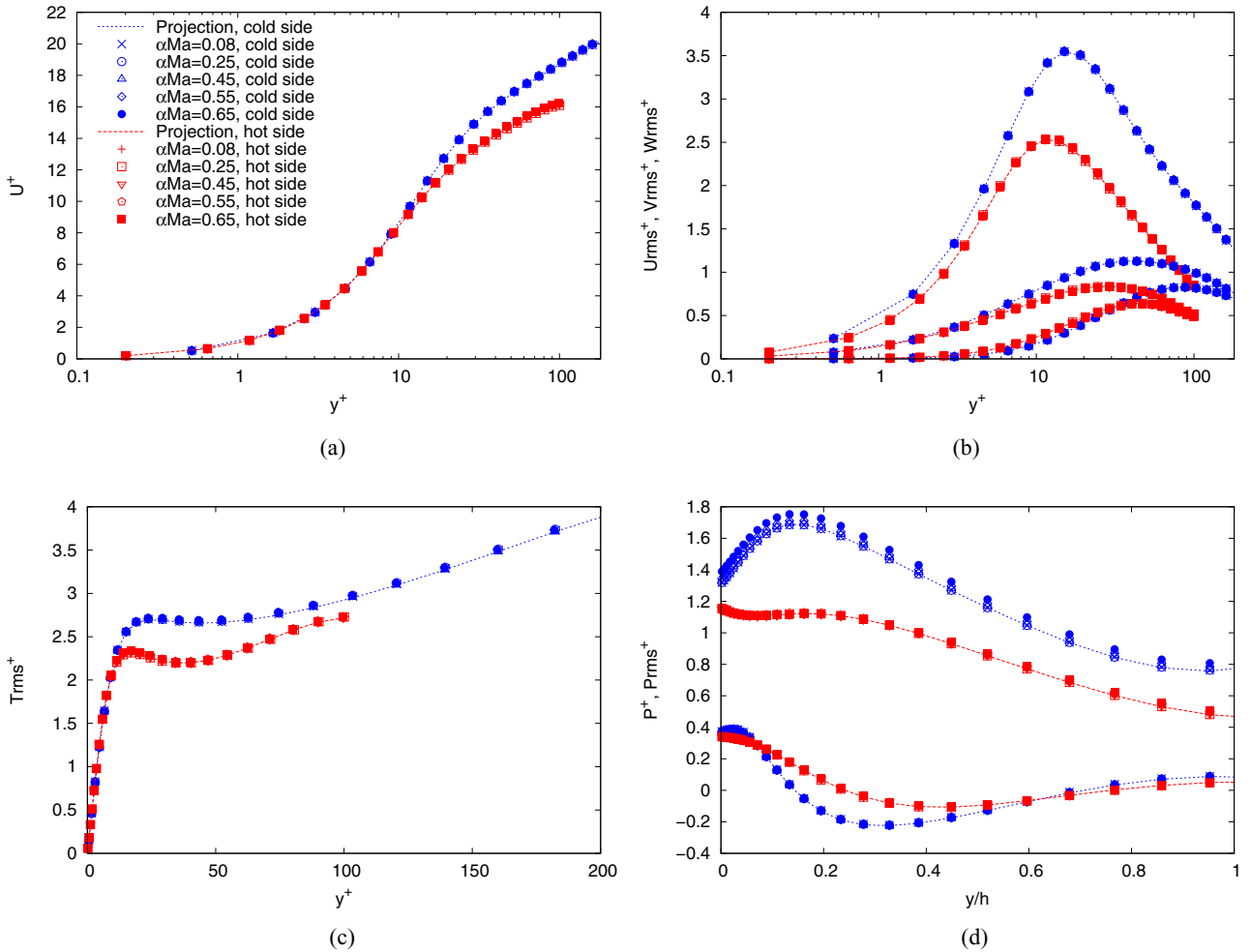


FIG. 1. Turbulence statistics for artificial compressibility simulations with the full formulation and the reference projection simulation in the case $Re_\tau = 180$ and $Pr = 0.76$. (a) Mean streamwise velocity. (b) From bottom to top: standard deviation of wall-normal velocity, of spanwise velocity, and of streamwise velocity. (c) Standard deviation of temperature. (d) From bottom to top: mean pressure and standard deviation of pressure.

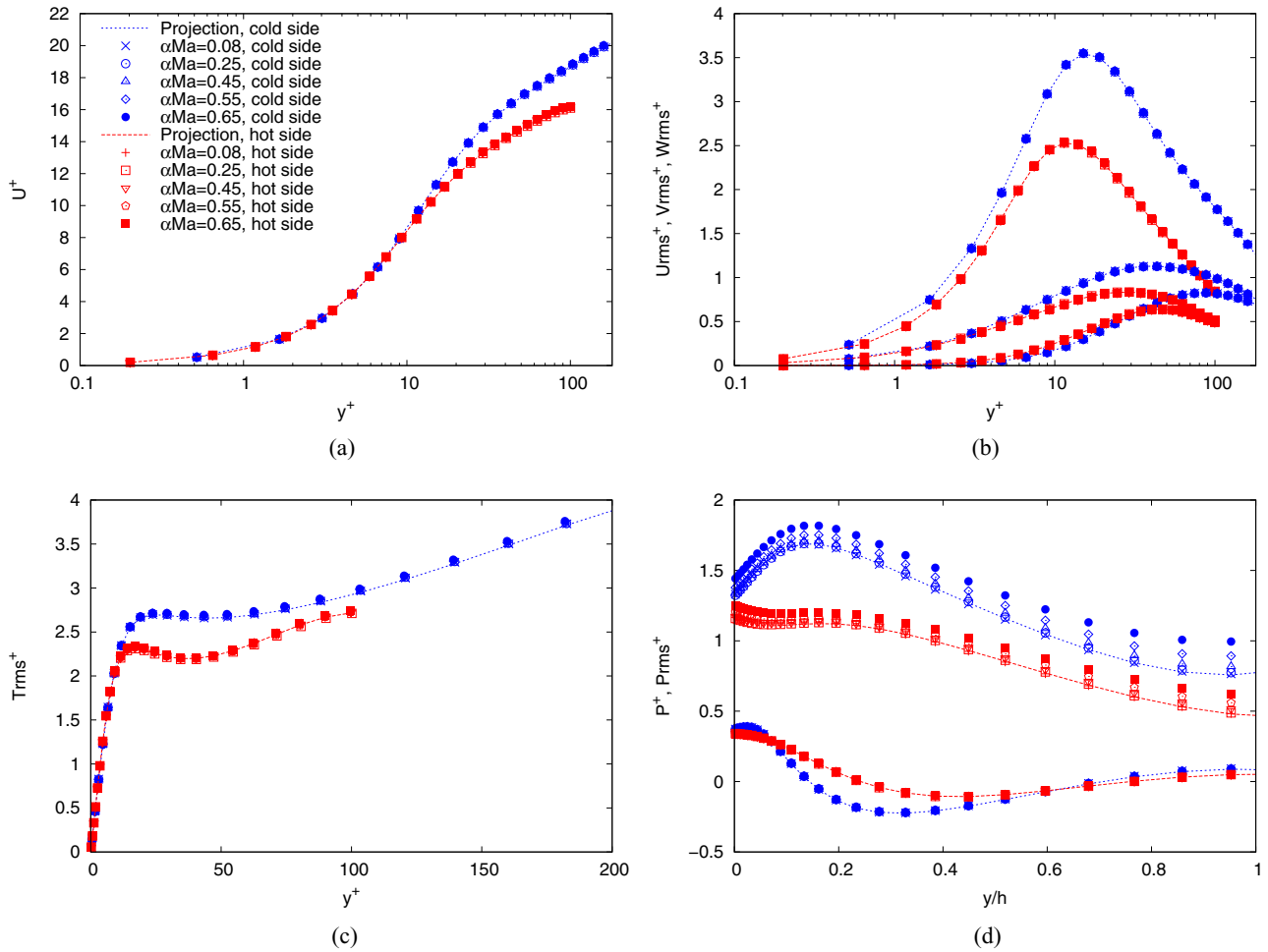


FIG. 2. Turbulence statistics for artificial compressibility simulations with the simplified formulation and the reference projection simulation in the case $Re_\tau = 180$ and $Pr = 0.76$. (a) Mean streamwise velocity. (b) From bottom to top: standard deviation of wall-normal velocity, of spanwise velocity, and of streamwise velocity. (c) Standard deviation of temperature. (d) From bottom to top: mean pressure and standard deviation of pressure.

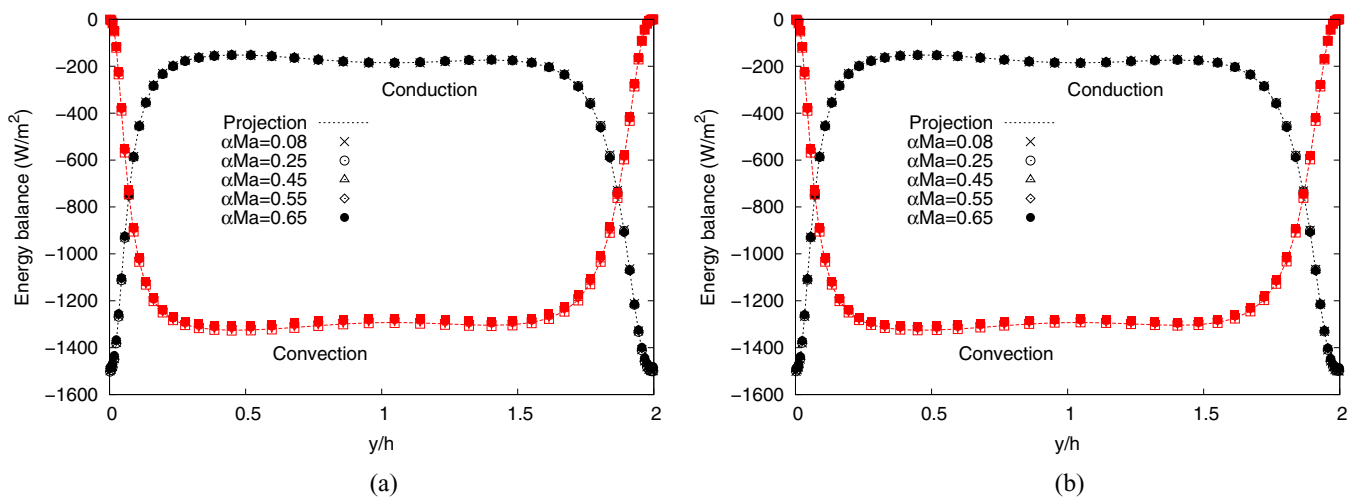


FIG. 3. Energy balance for artificial compressibility simulations with the full and simplified formulations in the case $Re_\tau = 180$ and $Pr = 0.76$, namely convective heat flux $\langle U_y(\gamma P_0)/(\gamma - 1) \rangle$ (“Convection”) and conductive heat flux $(-\lambda(\partial T/\partial y))$ (“Conduction”). (a) Full formulation. (b) Simplified formulation.

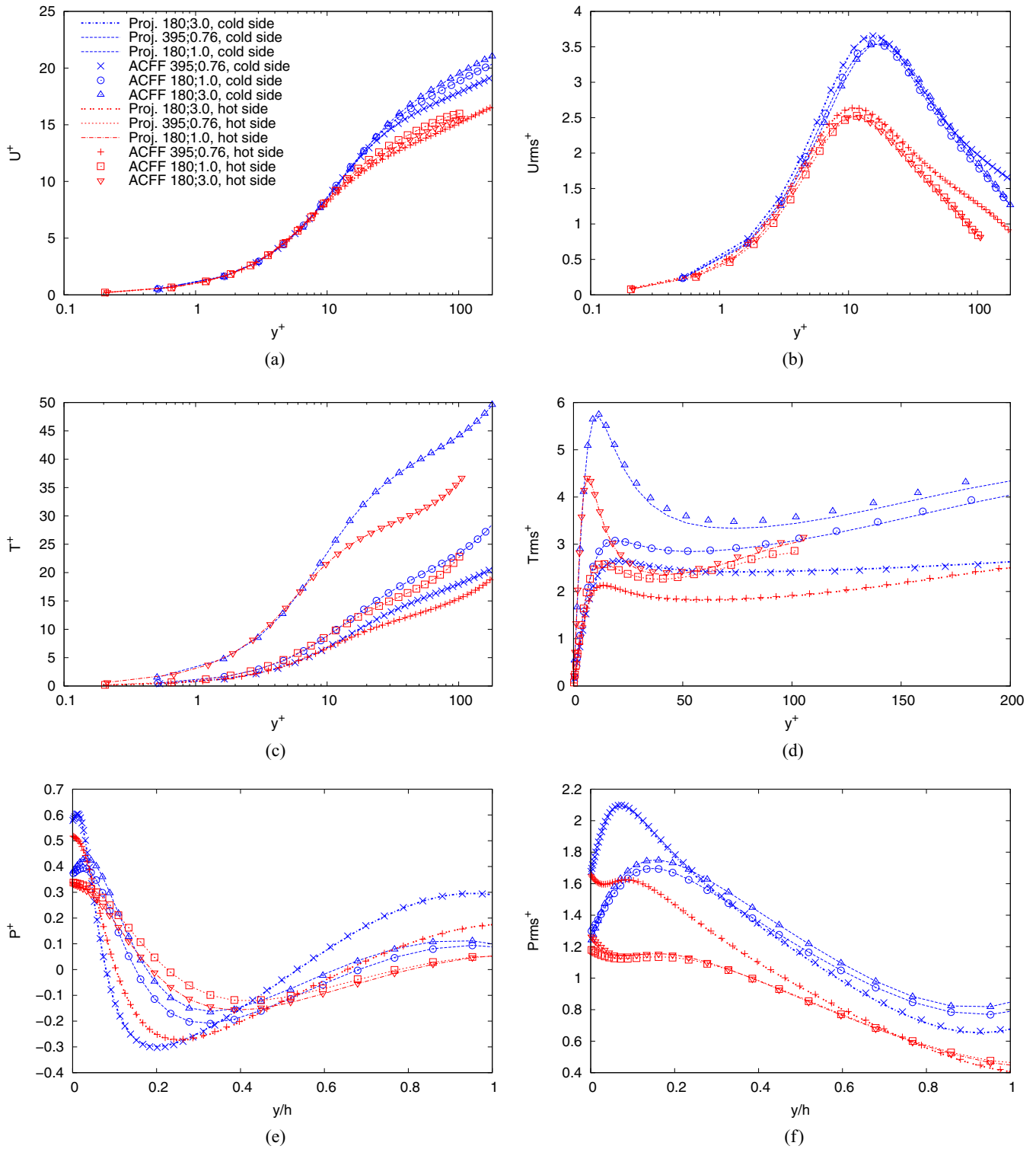


FIG. 4. Turbulence statistics for artificial compressibility simulations with the full formulation (ACFF) and the reference projection simulation (Proj.) in the cases $Re_\tau = 395$ and $Pr = 0.76$, $Re_\tau = 180$ and $Pr = 1.0$, and $Re_\tau = 180$ and $Pr = 3.0$. (a) Mean streamwise velocity. (b) Standard deviation of streamwise velocity. (c) Mean temperature. (d) Standard deviation of temperature. (e) Mean pressure. (f) Standard deviation of pressure.

is discretized with a third-order QUICK (quadratic upstream interpolation for convective kinetics) scheme [38]. At the walls, a no-slip boundary condition is used for velocity, and the temperature is imposed. No wall boundary condition is

required for the pressure. This is performed using the TRIOCFD software [39].

Three resolution algorithms are used. In the first reference algorithm, the low Mach number equations are resolved using

a projection method, a setup that has been validated extensively in the same configuration in previous papers [24–26]. In the second algorithm, referred to as “full formulation” hereafter, the flow is simulated using Eqs. (5)–(8) and (9). In the third algorithm, referred to as “simplified formulation” hereafter, we also use Eqs. (5)–(8) but neglect the dilatation term (III) in Eq. (9). Note that in both the projection method and the artificial compressibility methods, the mechanical pressure has a volume integral of zero at each time step. Let us first focus on the case $Re_\tau = 180$ and $Pr = 0.76$ in order to compare the full and simplified formulations and assess the influence of the artificial Mach number on the predictions. In that case, both the full formulation and the simplified formulation were found to be stable using our numerical setup. The results are presented in Fig. 1 for the full formulation and in Fig. 2 for the simplified formulation. In both the full formulation and the simplified formulation, the predictions provided by the artificial compressibility methods are, with a low artificial Mach number, almost identical to the reference projection simulation for all first-order and second-order statistics of turbulence. In particular, the simulations reproduce accurately the asymmetry between the hot and cold side of the channel, which results from the variation of the fluid properties with temperature. As evidenced by Fig. 3, the simulations also predict accurately the energy balance between the mean convective and conductive heat fluxes, which in a strongly anisothermal channel at low Mach number is given by

$$\langle U_y(\gamma P_0)/(\gamma - 1) \rangle = \langle \lambda(\partial T/\partial y) \rangle - \langle \lambda(\partial T/\partial y) \rangle_{y=0}. \quad (11)$$

This shows that the strong coupling between temperature and turbulence is correctly taken into account in the artificial compressibility methods and hence proves that the numerical simulation of anisothermal low Mach number flows with artificial pressure equations is possible. In addition, the volume-integral term (III) in Eq. (9) can be considered negligible given the small difference between the predictions of the full formulation and the simplified formulation. Neglecting this term as in the simplified formulation leaves only computationally inexpensive surface-integral terms in Eq. (9) and thus improves the efficiency of the numerical procedure. On the other hand, neglecting the volume-integral term (III) in Eq. (9) deteriorates the accuracy of the prediction for the standard deviation of pressure at larger artificial Mach numbers. Indeed, this quantity is one of the toughest to capture with artificial compressibility methods [18]. Using the full formulation, its profile remains very close to the reference projection profile until $\alpha Ma = 0.45$ (Fig. 1), whereas the discrepancy is larger using the simplified formulation (Fig. 2). Nevertheless, accurate results are obtained for all turbulence statistics at $\alpha Ma = 0.25$ with both methods. This implies in particular that the Nusselt number is well predicted. Numerically, the error on the Nusselt number is less than 1% even with the larger artificial Mach number of 0.65. The applicability of the artificial compressibility method at a larger Reynolds number ($Re_\tau = 395$) and larger Prandtl numbers ($Pr = 1.0$ or 3.0) is assessed in Fig. 4. In each configuration investigated, the method is able to produce accurate results for all first- and second-order turbulence statistics of velocity, temperature, and pressure.

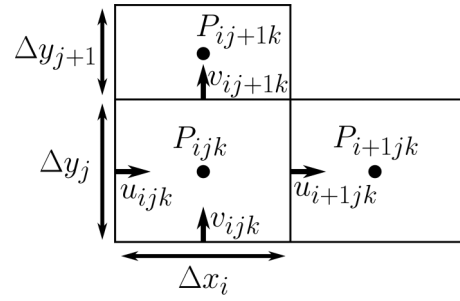


FIG. 5. Staggered grid system.

IV. CONCLUSION

The artificial compressibility method proposed in this paper is well suited to anisothermal low Mach number flows, even in the case of strong coupling between velocity and temperature. Thermal effects are accounted for using two pressures, namely a thermodynamic pressure and a mechanical pressure, similarly to using a low Mach number approximation [1]. The method can *a priori* be applied for any Reynolds and Prandtl numbers as no particular assumption regarding the Reynolds and Prandtl numbers is made in the theoretical derivation. Numerically, we assessed two friction Reynolds numbers (180 and 395) and three Prandtl numbers (0.76, 1.0, and 3.0). In all cases, the procedure is stable and provides accurate results for a strongly anisothermal channel flow. In particular, the procedure is able to predict the asymmetry between the profiles at the hot and cold sides of the channel caused by the coupling between temperature and velocity. The Nusselt number is predicted with an error of less than 1% even with the larger artificial Mach number of 0.65. Compared to the use of the compressible Navier-Stokes equations, it provides a speedup that depends on the physical Mach number of the configuration. Compared to a projection method, the method is local in space and can thus be easily parallelized.

ACKNOWLEDGMENTS

This work was funded by the French Investments for the future (“Investissements d’Avenir”) programme managed by the National Agency for Research (ANR) under Contract No. ANR-10-LABX-22-01 (labex SOLSTICE). The authors gratefully acknowledge the CEA for the development of the TRUST platform. This work was completed thanks to a grant of access to the HPC resources of CINES under the allocations 2020-A0042A05099 made by GENCI.

APPENDIX: NUMERICAL SCHEMES

This Appendix presents the implementation of the terms of the pressure evolution equation. Since we use a staggered grid system, velocity and pressure are not discretized at the same locations. This is illustrated in Fig. 5 in the two-dimensional case. The velocity divergence is discretized as

$$(\nabla \cdot U)_{i,j,k} = \frac{u_{i+1,j,k} - u_{i,j,k}}{\Delta x_i} + \frac{v_{i,j+1,k} - v_{i,j,k}}{\Delta y_j} + \frac{w_{i,j,k+1} - w_{i,j,k}}{\Delta z_k}. \quad (A1)$$

The convective term is discretized as

$$[\nabla \cdot (UP)]_{i,j,k} = \frac{u_{i+1,j,k}(P_{i+1,j,k} + P_{i,j,k}) - u_{i,j,k}(P_{i,j,k} + P_{i-1,j,k})}{2\Delta x_i} + \frac{v_{i,j+1,k}(P_{i,j+1,k} + P_{i,j,k}) - v_{i,j,k}(P_{i,j,k} + P_{i,j-1,k})}{2\Delta y_j} + \frac{w_{i,j,k+1}(P_{i,j,k+1} + P_{i,j,k}) - w_{i,j,k}(P_{i,j,k} + P_{i,j,k-1})}{2\Delta z_k}. \quad (A2)$$

The conductive term is discretized as

$$[\nabla \cdot (\lambda \nabla T)]_{i,j,k} = \frac{(\lambda_{i+1,j,k} + \lambda_{i,j,k}) \frac{T_{i+1,j,k} - T_{i,j,k}}{\Delta x_{i+1} + \Delta x_i} - (\lambda_{i,j,k} + \lambda_{i-1,j,k}) \frac{T_{i,j,k} - T_{i-1,j,k}}{\Delta x_i + \Delta x_{i-1}}}{\Delta x_i} + \frac{(\lambda_{i,j+1,k} + \lambda_{i,j,k}) \frac{T_{i,j+1,k} - T_{i,j,k}}{\Delta y_{j+1} + \Delta y_j} - (\lambda_{i,j,k} + \lambda_{i,j-1,k}) \frac{T_{i,j,k} - T_{i,j-1,k}}{\Delta y_j + \Delta y_{j-1}}}{\Delta y_j} + \frac{(\lambda_{i,j,k+1} + \lambda_{i,j,k}) \frac{T_{i,j,k+1} - T_{i,j,k}}{\Delta z_{k+1} + \Delta z_k} - (\lambda_{i,j,k} + \lambda_{i,j,k-1}) \frac{T_{i,j,k} - T_{i,j,k-1}}{\Delta z_k + \Delta z_{k-1}}}{\Delta z_k}. \quad (A3)$$

-
- [1] S. Paolucci, On the filtering of sound from the Navier-Stokes equations, Technical Report SAND82-8257, Sandia National Labs., Livermore, CA (1982).
 - [2] A. J. Chorin, Numerical solution of the Navier-Stokes equations, *Math. Comput.* **22**, 745 (1968).
 - [3] R. Temam, Sur l'approximation de la solution des équations de Navier-Stokes par la méthode des pas fractionnaires (ii), *Arch. Ration. Mech. Anal.* **33**, 377 (1969).
 - [4] R. Benzi, S. Succi, and M. Vergassola, The lattice boltzmann equation: Theory and applications, *Phys. Rep.* **222**, 145 (1992).
 - [5] A. J. Chorin, A numerical method for solving incompressible viscous flow problems, *J. Comput. Phys.* **2**, 12 (1967).
 - [6] T. Ohwada and P. Asinari, Artificial compressibility method revisited: Asymptotic numerical method for incompressible navier-stokes equations, *J. Comput. Phys.* **229**, 1698 (2010).
 - [7] P. J. O'Rourke and F. V. Bracco, Two scaling transformations for the numerical computation of multidimensional unsteady laminar flames, *J. Comput. Phys.* **33**, 185 (1979).
 - [8] J. D. Ramshaw, P. J. O'Rourke, and L. R. Stein, Pressure gradient scaling method for fluid flow with nearly uniform pressure, *J. Comput. Phys.* **58**, 361 (1985).
 - [9] Y. Wang and A. Trounev, Artificial acoustic stiffness reduction in fully compressible, direct numerical simulation of combustion, *Combust. Theor. Modell.* **8**, 633 (2004).
 - [10] S. Ansumali, I. V. Karlin, and H. C. Öttinger, Thermodynamic Theory of Incompressible Hydrodynamics, *Phys. Rev. Lett.* **94**, 080602 (2005).
 - [11] I. V. Karlin, A. G. Tomboulides, C. E. Frouzakis, and S. Ansumali, Kinetically reduced local Navier-Stokes equations: An alternative approach to hydrodynamics, *Phys. Rev. E* **74**, 035702(R) (2006).
 - [12] M. Salinas-Vázquez, W. Vicente, E. Barrios, E. Martínez, A. Palacio, and A. Rodríguez, A low-mach number method for the numerical simulation of complex flows, *Appl. Math. Modell.* **37**, 9132 (2013).
 - [13] J. R. Clausen, Entropically damped form of artificial compressibility for explicit simulation of incompressible flow, *Phys. Rev. E* **87**, 013309 (2013).
 - [14] A. Toutant, General and exact pressure evolution equation, *Phys. Lett. A* **381**, 3739 (2017).
 - [15] S. Borok, S. Ansumali, and I. V. Karlin, Kinetically reduced local Navier-Stokes equations for simulation of incompressible viscous flows, *Phys. Rev. E* **76**, 066704 (2007).
 - [16] A. Toutant, Numerical simulations of unsteady viscous incompressible flows using general pressure equation, *J. Comput. Phys.* **374**, 822 (2018).
 - [17] A. Kajzer and J. Pozorski, Application of the entropically damped artificial compressibility model to direct numerical simulation of turbulent channel flow, *Comput. Math. Appl.* **76**, 997 (2018).
 - [18] D. Dupuy, A. Toutant, and F. Bataille, Analysis of artificial pressure equations in numerical simulations of a turbulent channel flow, *J. Comput. Phys.* **411**, 109407 (2020).
 - [19] S. Serra, A. Toutant, and F. Bataille, Thermal large eddy simulation in a very simplified geometry of a solar receiver, *Heat Transf. Eng.* **33**, 505 (2012).
 - [20] X. Daguene-Frick, J.-M. Foucaut, S. Coudert, A. Toutant, and G. Olalde, Experimental analysis of the turbulent flow behavior of a textured surface proposed for asymmetric heat exchangers, *Flow Turb. Combust.* **89**, 149 (2012).
 - [21] X. Daguene-Frick, A. Toutant, F. Bataille, and G. Olalde, Numerical investigation of a ceramic high-temperature pressurized-air solar receiver, *Solar Energy* **90**, 164 (2013).
 - [22] A. Colleoni, A. Toutant, G. Olalde, and J.-M. Foucaut, Optimization of winglet vortex generators combined with riblets for wall/fluid heat exchange enhancement, *Appl. Therm. Eng.* **50**, 1092 (2013).
 - [23] S. Serra, A. Toutant, F. Bataille, and Y. Zhou, High-temperature gradient effect on a turbulent channel flow using thermal large-eddy simulation in physical and spectral spaces, *J. Turb.* **13**, N49 (2012).
 - [24] A. Toutant and F. Bataille, Turbulence statistics in a fully developed channel flow submitted to a high temperature gradient, *Int. J. Therm. Sci.* **74**, 104 (2013).
 - [25] D. Dupuy, A. Toutant, and F. Bataille, Turbulence kinetic energy exchanges in flows with highly variable fluid properties, *J. Fluid Mech.* **834**, 5 (2018).

- [26] D. Dupuy, A. Toutant, and F. Bataille, Effect of the Reynolds number on turbulence kinetic energy exchanges in flows with highly variable fluid properties, *Phys. Fluids* **31**, 015104 (2019).
- [27] P.-L. Lions and T. H. Moulden, *Mathematical Topics in Fluid Mechanics, Vol. 1: Incompressible Models* (Oxford University Press, New York, 1996).
- [28] C. D. Munz, M. Dumbser, and M. Zucchini, The multiple pressurevariables method for fluid dynamics and aeroacoustics at low mach numbers, in *Numerical methods for Hyperbolic and Kinetic Problems*, IRMA lectures in Mathematics and Theoretical Physics Vol. 7 (European Mathematical Society Publishing House, 2005), p. 335.
- [29] A. Meister, Asymptotic single and multiple scale expansions in the low mach number limit, *SIAM J. Appl. Math.* **60**, 256 (1999).
- [30] Y. Huang and H. H. Bau, Thermoacoustic waves in a confined medium, *Int. J. Heat Mass Transf.* **40**, 407 (1997).
- [31] S. Sarkar, The pressure-dilatation correlation in compressible flows, *Phys. Fluids A* **4**, 2674 (1992).
- [32] F. Nicoud, Conservative high-order finite-difference schemes for low-Mach number flows, *J. Comput. Phys.* **158**, 71 (2000).
- [33] J. H. Williamson, Low-storage Runge-Kutta schemes, *J. Comput. Phys.* **35**, 48 (1980).
- [34] D. Dupuy, A. Toutant, and F. Bataille, Study of the large-eddy simulation subgrid terms of a low mach number anisothermal channel flow, *Int. J. Therm. Sci.* **135**, 221 (2018).
- [35] D. Dupuy, A. Toutant, and F. Bataille, A priori tests of subgrid-scale models in an anisothermal turbulent channel flow at low mach number, *Int. J. Therm. Sci.* **145**, 105999 (2019).
- [36] D. Dupuy, A. Toutant, and F. Bataille, A posteriori tests of subgrid-scale models in an isothermal turbulent channel flow, *Phys. Fluids* **31**, 045105 (2019).
- [37] D. Dupuy, A. Toutant, and F. Bataille, A posteriori tests of subgrid-scale models in an anisothermal turbulent channel flow at low mach number, *Phys. Fluids* **31**, 065113 (2019).
- [38] B. P. Leonard, A stable and accurate convective modeling procedure based on quadratic upstream interpolation, *Comput. Methods Appl. Mech. Eng.* **19**, 59 (1979).
- [39] C. Calvin, O. Cueto, and P. Emonot, An object-oriented approach to the design of fluid mechanics software, *ESAIM: Math. Modell. Numer. Anal.* **36**, 907 (2002).